HHS Public Access

Author manuscript

Neurobiol Dis. Author manuscript; available in PMC 2017 November 01.

Published in final edited form as:

Neurobiol Dis. 2016 November ; 95: 238–249. doi:10.1016/j.nbd.2016.07.020.

Live imaging of mitochondrial dynamics in CNS dopaminergic neurons *in vivo* demonstrates early reversal of mitochondrial transport following MPP+ exposure

April A. Dukes[1,2], **Qing Bai**[1,2], **Victor S. Van Laar**[1,2], **Yangzhong Zhou**[1,2,3], **Vladimir Ilin**[1,2], **Christopher N. David**[1,2,4], **Zeynep S. Agim**[5], **Joshua L. Bonkowsky**[6], **Jason R. Cannon**[5], **Simon C. Watkins**[7,8], **Claudette M. St. Croix**[7,9], **Edward A. Burton**[1,2,10,11,*], and **Sarah B. Berman**[1,2,*]

[1]Pittsburgh Institute for Neurodegenerative Diseases, University of Pittsburgh, Pittsburgh, PA, USA

[2]Department of Neurology, University of Pittsburgh, Pittsburgh, PA, USA

[3]Tsinghua University Medical School, Beijing, China

[4]MSTP program, University of Pittsburgh School of Medicine, Pittsburgh, PA, USA

[5]School of Health Sciences, Purdue University, West Lafayette, IN, USA

[6]Department of Pediatrics, University of Utah School of Medicine, Salt Lake City, UT, USA

[7]Center for Biologic Imaging, University of Pittsburgh, Pittsburgh, PA, USA

[8]Department of Cell Biology, University of Pittsburgh, Pittsburgh, PA, USA

[9]Department of Environmental and Occupational Health, University of Pittsburgh, Pittsburgh, PA, USA

[10]Department of Microbiology and Molecular Genetics, University of Pittsburgh, Pittsburgh, PA, USA

[11]Geriatric Research, Education and Clinical Center, Pittsburgh Veterans' Affairs Healthcare System, Pittsburgh, PA, USA

Abstract

Extensive convergent evidence collectively suggests that mitochondrial dysfunction is central to the pathogenesis of Parkinson's disease (PD). Recently, changes in the dynamic properties of mitochondria have been increasingly implicated as a key proximate mechanism underlying neurodegeneration. However, studies have been limited by the lack of a model in which mitochondria can be imaged directly and dynamically in dopaminergic neurons of the intact

*Address for correspondence: Edward A. Burton, 7015 BST-3, 3501 5th Ave, Pittsburgh, PA 15213, eab25@pitt.edu, or: Sarah B. Berman, 7037 BST-3, 3501 5the Ave, Pittsburgh, PA 15213, bermans@upmc.edu.

vertebrate CNS. We generated transgenic zebrafish in which mitochondria of dopaminergic neurons are labeled with a fluorescent reporter, and optimized methods allowing direct intravital imaging of CNS dopaminergic axons and measurement of mitochondrial transport *in vivo*. The proportion of mitochondria undergoing axonal transport in dopaminergic neurons decreased overall during development between 2 days post-fertilization (dpf) and 5dpf, at which point the major period of growth and synaptogenesis of the relevant axonal projections is complete. Exposure to 0.5 – 1.0mM MPP^+ between 4 – 5 dpf did not compromise zebrafish viability or cause detectable changes in the number or morphology of dopaminergic neurons, motor function or monoaminergic neurochemistry. However, 0.5mM MPP^+ caused a 300% increase in retrograde mitochondrial transport and a 30% decrease in anterograde transport. In contrast, exposure to higher concentrations of MPP^+ caused an overall reduction in mitochondrial transport. This is the first time mitochondrial transport has been observed directly in CNS dopaminergic neurons of a living vertebrate and quantified in a PD model *in vivo*. Our findings are compatible with a model in which damage at presynaptic dopaminergic terminals causes an early compensatory increase in retrograde transport of compromised mitochondria for degradation in the cell body. These data are important because manipulation of early pathogenic mechanisms might be a valid therapeutic approach to PD. The novel transgenic lines and methods we developed will be useful for future studies on mitochondrial dynamics in health and disease.

Introduction

Dysregulation of the dynamic properties of mitochondria (including axonal transport, fission, fusion, biogenesis, and degradation) in disease-susceptible neuronal groups has been implicated as an upstream event in the pathogenesis of Parkinson's disease (PD) (Burte et al., 2015; Haddad and Nakamura, 2015; Van Laar and Berman, 2013). Loss of function mutations of the PARK2 (Kitada et al., 1998) and PARK6 (Valente et al., 2004) genes cause familial Parkinsonism phenocopies; these genes encode Parkin and PINK1 respectively, both of which are centrally involved in regulating mitochondrial dynamics and homeostasis (Deng et al., 2008; Exner et al., 2007; Lutz et al., 2009; Narendra et al., 2008; Narendra et al., 2010; Poole et al., 2008). Furthermore, both environmental toxicants linked to elevated risk of PD (Tanner et al., 2011) and chemicals known to cause degeneration of dopaminergic neurons and acute Parkinsonism in humans (Langston et al., 1983), regulate mitochondrial trafficking, fission and fusion *in vitro* (Arnold et al., 2011; Barsoum et al., 2006; Wang et al., 2011).

We previously developed methodology allowing quantification of mitochondrial fission, fusion, and transport in living cultured neurons (Berman et al., 2009). Using this approach, we demonstrated alterations in mitochondrial dynamics that correlated with the earliest pathological changes in neurites following chronic sub-lethal exposure to rotenone (Arnold et al., 2011). Importantly, static indices of mitochondrial morphology were largely uninformative concerning the complex series of dynamic changes that we observed through live imaging. This suggests that static imaging modalities offer an inadequate picture of the events underlying pathogenesis. It is therefore critically important to evaluate mitochondrial dynamics using a dynamic imaging modality, such as direct observation or time-lapse imaging.

Parkinson's disease pathology affects neurons selectively, suggesting that the relevant pathogenic mechanisms may be unique to vulnerable cellular populations. The specific cell-autonomous and non-autonomous factors governing selective neuronal vulnerability of neurons in PD are not fully understood and have not yet been replicated *in vitro*. Consequently, in order to understand the role of mitochondrial dynamics in PD pathogenesis, it would be highly desirable to carry out dynamic imaging of mitochondria directly in relevant neuronal groups (such as dopaminergic neurons) of the intact CNS. Several different hypotheses concerning the contribution of mitochondrial dynamics to the pathogenesis of PD could be tested directly using such technology. For example, it is possible that generalized systemic perturbations – such as loss of Parkin or PINK1, or exposure to rotenone – cause specific pathology by provoking disproportionately severe, or qualitatively different, responses in dopaminergic neurons compared with non-susceptible cell groups. However, dynamic, *in vivo* imaging of mitochondria in PD-vulnerable neuronal populations has not previously been possible.

Zebrafish provide an opportunity for imaging dopaminergic neurons in the intact CNS of a living vertebrate organism. Zebrafish models have been exploited previously to study the pathogenesis of Parkinson's disease, and several lines of evidence suggest that zebrafish PD models have both construct and face validity. Zebrafish share highly conserved orthologs of human genes involved in PD pathogenesis, including those encoding proteins known to function in regulating mitochondrial dynamics (Bai et al., 2006; Flinn et al., 2009; Flinn et al., 2013; Milanese et al., 2012). The CNS dopaminergic system of zebrafish is complex, and includes a putative anatomical homologue of the mammalian nigrostriatal projection (Rink and Wullimann, 2001). Dopaminergic function in zebrafish regulates spontaneous movement (Farrell et al., 2011). Finally, zebrafish dopaminergic neurons are susceptible to chemical toxicants, such as MPTP, that are often used to model Parkinsonism in mammalian models and which have been implicated in causing Parkinsonism in humans (Farrell et al., 2011; Lam et al., 2005; McKinley et al., 2005; Sallinen et al., 2010; Sallinen et al., 2009; Wen et al., 2008). Importantly for live imaging studies, larvae can be manipulated to be transparent (White et al., 2008) and are viable immobilized on the stage of a confocal microscope, allowing direct imaging of fluorescent reporters. Furthermore, generation of suitable stable transgenic lines is now facile and several regulatory constructs are available that express transgenes in CNS dopaminergic neurons (Bai and Burton, 2009; Fujimoto et al., 2011; Xi et al., 2011).

We generated novel transgenic zebrafish lines, in which mitochondria of dopaminergic neurons were labeled with fluorescent reporters, and used time-lapse imaging to measure mitochondrial axonal transport in dopaminergic neurons during development. We found that exposure to low concentrations of the PD-relevant mitochondrial inhibitor MPP^+ caused a dramatic and early reversal in axonal mitochondrial flux, which preceded any detectable loss of dopaminergic neurons, neurochemical abnormalities or neurobehavioral deficits.

Methods

Zebrafish

All studies were carried out in full compliance with federal and local regulations, in accordance with NIH guidelines for animal care and use, and with approval from the University of Pittsburgh Institutional Animal Care and Use Committee. Zebrafish larvae were generated by crossing adult WT (strain AB), Casper (genotype: *roy*$^{-/-}$; *nacre*$^{-/-}$) (White et al., 2008), or Tg(*otpb:gal4-vp16,myl7:gfp*)^{zc57} (referred to as Tg(*otpb:gal4*) for brevity) (Fujimoto et al., 2011) zebrafish. Embryos were raised at 28.5°C in a light/dark cycle (14 hours light:10 hours dark; illumination at 200 Lux; white light color temperature 3700K) in E3 buffer (5mM NaCl, 0.17mM KCl, 0.33mM $CaCl_2$, 0.33mM $MgSO_4$; unless otherwise stated, all chemicals were supplied by Sigma, St. Louis, MO). For MPP^+ exposures, 4dpf zebrafish were placed in E3 buffer containing MPP^+ at the final concentrations indicated in the figures, for 16 hours at 28.5°C, then washed 3 times in E3 and allowed to recover for at least 1 hour in E3 prior to further experimentation.

Generation of pT2- mtPAGFP-mtdsRed2 transgene construct

The SV40 polyA signal of pT2-5UASMCS (a gift from Dr. Koichi Kawakami, NIG, Japan) (Asakawa et al., 2008) was replaced with the HSV *tk* polyA signal, then the 5 x UAS was deleted to yield pT2-E1b-HSVtkPolyA. Sequence encoding mitochondrially-targeted DsRed2 (mtDsRed2) was amplified from pDsRed2-Mito (Clontech) using primers 5′-GGA ATT CCG CTA GCA TGT CCG TCC-3′ and 5′-CCG CTC GAG CTA CAG GAA CAG GTG GT-3′ to introduce EcoRI/XhoI restriction sites, and the fragment was inserted into the EcoRI/XhoI sites of pT2-E1b-HSVtkpolyA to yield pT2-E1b:mtDsRed2-HSVtkpolyA. Mitochondrially-targeted photoactivatable GFP (mtPAGFP) was amplified from mito-PAGFP (Karbowski et al., 2004; Patterson and Lippincott-Schwartz, 2002) (a gift from Dr. Richard Youle, NINDS, Bethesda, MD) using primers 5′-GGA ATT CCG CTA GCA TGT CCG TCC-3′ and 5′-CCG CTC GAG CCG CTT TAC TTG TAC AGC-3′ to introduce EcoRI/XhoI restriction sites and the fragment was inserted into the EcoRI/XhoI sites of pT2-5UASMCS to yield pT2-5UAS:mtPAGFP. Finally an SphI fragment from pT2-E1b:mtDsRed2-HSVtkpolyA was inserted into the SphI site of pT2-5UAS:mtPAGFP to yield pT2-5UAS:mtPAGFP:mtDsRed2. The plasmid was fully verified by DNA sequencing and expression of both fluorescent markers was confirmed by co-transfection of HEK 293T cells with pT2-5UAS:mtPAGFP:mtDsRed2 and a Gal4-VP16 expressing plasmid. Transfected cells showed dsRed2-labeled mitochondria that could be photo-activated to show GFP fluorescence (not shown).

Transgenic zebrafish

Transgenic lines were derived exactly as described in our previous work (Bai and Burton, 2009; Bai et al., 2007; Bai et al., 2014), except that we employed the Tol2 method for transgenesis (Asakawa et al., 2008; Kawakami et al., 2004). Tg(*otpb:gal4*); *roy*$^{-/-}$; *nacre*$^{-/-}$ embryos were injected at the 1-cell stage with 1-2 nL of transgene solution (pT2-5UAS:mtPAGFP:mtDsRed2 plasmid, 25 μg/μL; 0.5% phenol red; 240mM KCl; 40mM 4-(2-hydroxyethyl)-1-piperazineethanesulfonic acid, pH 7.4; *tol2* transposase mRNA, 50 ng/μL; nuclease-free H_2O). Surviving embryos were screened for diencephalic mtDsRed2

expression at 72 hours post-fertilization and raised to sexual maturity. Mosaic F0 chimeras that could transmit the UAS:mtDsRed2: mtPAGFP transgene through the germline were identified by mtDsRed2 expression in their F1 progeny. Multiple F1 founders were screened to identify lines with robust transactivation of the transgene by Gal4. The lines reported here were expanded from a single F1 founder; the transgenes showed stable Mendelian inheritance over multiple generations indicating a single integration site, and were selected for minimal variegation.

Imaging

Tg(*otpb:Gal4*); Tg(*UAS:mtPAGFP:mtDsRed2*) zebrafish larvae at 2 – 5 dpf were immobilized in 0.015% tricaine and mounted in isotonically buffered CyGEL™ (Biostatus, Shepshed, UK) containing 0.03% tricaine in a 35mm glass bottom dish (MatTek, Ashland, MA), oriented so that one dorsolateral side was flush against the glass. Time-lapse images were obtained with a Nikon TI inverted microscope equipped with a swept field confocal head. 3D stacks were collected over time with a 1.15 NA 40x water immersion objective lens using Nikon NIS-Elements software. Images of the mitochondria within the diencephalospinal tracts were acquired as 3-8 Z-plane images every 10 seconds for 10 minutes. A single DIC image was obtained in the center of the stack to document the imaging location. Photoactivation and image acquisition in figures 1 and 2 was carried out using an Olympus IX81 inverted microscope with FV1000 laser scanning confocal system. mtPAGFP was photoactivated within defined regions of interest by excitation at 405 nm (Arnold et al., 2011).

Analysis of Mitochondrial Movement

Time-lapse image series were analyzed using Imaris 8.1 software (Bitplane, South Windsor, CT). Images were stabilized and a binary threshold applied so that mitochondrial were clearly visible. All mitochondria (including those present in the first frame and those that entered the imaging area during acquisition) were identified manually in each frame. The x, y and z coordinates of each mitochondrion in each frame were then exported to MATLAB®, and further analysis performed using custom scripts that calculated total displacement, direction, velocity, and proportion of frame transitions at which a displacement occurred for each mitochondrion (scripts are available from the authors on request). All zebrafish were imaged in the same orientation so that retrograde and anterograde movements could be distinguished by the polarity of x-plane displacements. Distance was calculated as the sum of each frame-to-frame displacement above a noise threshold (2μm), regardless of direction. Velocity of retrograde and anterograde movements was calculated as the distance moved in the appropriate direction divided by the time spent moving in that direction (defined by the number of frame transitions during which displacements in appropriate direction occurred). % time moving was calculated as the proportion of frame transitions at which displacement above threshold was detected.

Measurement of dopamine and serotonin levels

Sample collection and analysis were similar to our previous work (Milanese et al., 2012). Briefly, 5dpf zebrafish were sonicated in 0.4M perchloric acid at 4°C after removal of excess E3. Lysates were centrifuged at 17,000*g* at 4°C, and the supernatant filtered through a 0.22-

μm nylon membrane. 25μL of supernatant was injected into Dionex Ultimate 3000 (ThermoScientific, Germany) chromatography system with an auto-sampler maintained at 4°C. The mobile phase consisted of 80mM NaH_2PO_4, 10% methanol, 2mM octanesulfonic acid, 0.025mM ethylenediaminetetraacetic acid and 0.2mM triethylamine, pH 2.4. Analytes were separated at 32°C at a flow rate of 0.6 mL/min on a Waters XBridge reverse phase C18 column (150 × 3.0mm, 3.0μm particle size) (Waters Corp, Ireland), and detected using a Coulochem III (ThermoScientific) electrochemical detector. The electrochemical potential of the detector was 350mV, with a guard cell at 450mV and a conditioning cell at −150mV. Dopamine and serotonin concentrations were calculated from peak height and area under the curve by comparison with a standard curve. Neurotransmitter amounts are shown as pg/animal.

Zebrafish motor function

Zebrafish locomotor behavioral testing was performed exactly as described in our previous work (Farrell et al., 2011; Zhou et al., 2014). Briefly, 5dpf zebrafish larvae were placed in the wells of a black-walled 96-well plate with an optical glass bottom, and imaged in a 28.5°C incubator under bright white illumination (brightness 200 Lux, color temperature 3500K). Zebrafish motion in the resulting videos analyzed using the MATLAB® scripts *LSRtrack* and *LSRanalyze* (Cario et al., 2011). All data were derived from recordings in which there were < 5% total tracking errors.

Whole Mount Immunohistochemistry

Zebrafish were fixed in 4% paraformaldehyde (PFA) at 4°C for 16 hours, washed in phosphate buffered saline (PBS), and then dissected to expose the brain. The dissected zebrafish were washed in PBS + 0.3% Triton (PBST), treated with acetone for 10 minutes at −20°C, washed with PBST and then blocked overnight in PBS-T + 1% DMSO + 4% normal goat serum (NGS) at 4°C. After blocking, zebrafish were incubated in primary antibodies to TH (rabbit polyclonal, Millipore, cat # AB152; 1:1000) or GFP (chicken polyclonal, Abcam, Cat # AB13970; 1:5000) for 16 hours at 4°C. Following incubation in secondary antibody (AlexaFluor 488 goat-anti-rabbit IgG, AlexaFluor 488-goat-anti-chicken IgG, or AlexaFluor 647 goat-anti-rabbit IgG, Invitrogen; 1:1000), for 16 hours at 4°C in the dark, zebrafish were washed in PBS, and passed through a series of successively higher concentrations of glycerol to 80% for imaging.

Statistical analysis

Data comparing mitochondrial velocities, mitochondrial percentage of time mobile, zebrafish heart rate, dopamine and serotonin levels, and zebrafish velocity were analyzed using one-way analysis of variance with Tukey's test for post hoc pairwise comparisons. DA neuron counts were analyzed by Student's t test. Data comparing the percentage of mitochondria moving and proportion of mitochondria moving in anterograde or retrograde directions were analyzed by z test for proportions with Bonferroni correction for multiple comparisons.

Results

Transgenic zebrafish for imaging mitochondrial dynamics in dopaminergic neurons in vivo

We developed novel transgenic zebrafish lines in order to visualize mitochondria within the dopaminergic neurons of an intact vertebrate CNS. Lines were made on the *Casper* (genotype: *roy*$^{-/-}$; *nacre*$^{-/-}$) background that lacks pigment formation, to facilitate imaging studies (White et al., 2008). We employed Gal4/UAS genetics (Asakawa et al., 2008; Distel et al., 2009; Scheer and Campos-Ortega, 1999) to allow subsequent expression of transgenes in different neuronal populations or tissues, by use of appropriate Gal4 driver lines. For the present study, we used a Tg(*otpb:gal4*) driver line, in which Gal4 is expressed in ventral diencephalic dopaminergic neurons of the zebrafish CNS (Fujimoto et al., 2011). The method that we developed previously for unequivocal identification of mitochondrial fission and fusion in cultured cells depends on simultaneous expression of two fluorescent markers in mitochondria – a constitutive red fluorescent protein (mtDsRed2) and a photoactivatable green fluorescent protein (mtPAGFP) (Berman et al., 2009). In order to maximize the potential utility of the transgenic lines for measuring a range of mitochondrial dynamic properties in future studies, we developed a construct that expresses both proteins in the same cells of transgenic zebrafish by transcription from a UAS-bidirectional promoter fusion (figure 1A, B). Transient expression of the UAS:mtPAGFP:mtDsRed2 construct in Tg(*otpb:gal4*) zebrafish resulted in mitochondrial localization of both proteins in diencephalic neurons and their axons, and confirmed that the mtPAGFP marker could be selectively photoactivated in individual mitochondria (figure 1C). By time-lapse confocal imaging, it was possible to visualize mitochondrial transport (displacement of mtDsRed2-labeled mitochondria from one image in a time series to the next; figure 1D), mitochondrial fission (division of a mtDsRed2-labeled mitochondrion into two parts; figure 1E) and mitochondrial fusion (coalescence of a mt-DsRed2-labeled mitochondrion with a photoactivated mtPAGFP-labeled mitochondrion; Figure 1E), confirming that the method is effective *in vivo*. For the present work, we focused on evaluation of mitochondrial transport using the mt-DsRed2 reporter.

We established four independent stable transgenic Tg(*otpb:gal4*); Tg(*UAS:mtPAGFP:mtDsRed2*); *nacre*$^{-/-}$; *roy*$^{-/-}$ lines. We confirmed that these expressed the two fluorescent mitochondrial markers in dopaminergic neurons of the ventral diencephalon, identified by their anatomical location (figure 2A) and co-expression of tyrosine hydroxylase (TH; figure 2B). We also verified that the mtPAGFP marker in these stable lines could be photoactivated, both in neuronal cell bodies deep in the diencephalon (figure 2C) and in their axons in the spinal cord (2D). For further studies, we selected the line that showed the most robust and specific transgene expression, minimal variegation over multiple generations, and a Mendelian ratio of transgenic and non-transgenic offspring indicating a single transgene insertion. The lines have now been propagated beyond the F4 generation and continue to show stable transgene expression.

Mitochondrial transport in dopaminergic neurons during development

To evaluate mitochondrial axonal transport in dopaminergic neurons we took advantage of the anatomical configuration of the zebrafish dopaminergic system. Dopaminergic neurons

that project to the basal forebrain in zebrafish, which are thought to represent the anatomical homologue of the mammalian nigrostriatal system, reside in the ventral diencephalon (Rink and Wullimann, 2001). These neurons also send a caudal projection to the spinal cord (Tay et al., 2011). Axons of the dopaminergic diencephalospinal tract lie superficially within the spinal cord, facilitating live imaging by confocal microscopy. Furthermore, these axons run a linear rostro-caudal course, so that a significant axonal length can be imaged within a single microscopic field and a small number of confocal planes, and the direction of mitochondrial movement (anterograde versus retrograde) is easily determined. The Tg(*otpb:gal4*) driver line we employed expresses in groups DC4 and DC5 (Fujimoto et al., 2011) and has previously been employed in functional studies of the dopaminergic diencephalospinal tract (Lambert et al., 2012). By imaging axons of the proximal diencephalospinal tract every 10 seconds for 10 minutes in live immobilized *roy*$^{-/-}$; *nacre*$^{-/-}$; Tg(*otpb:gal4*); Tg(*UAS:mtPAGFP:mtDsRed2*) zebrafish, we were able to identify mitochondria in several axons simultaneously and to measure how their locations changed from one image to the next (figure 3A; and *methods*).

Inspection of the image series showed that there were both stationary and motile mitochondria. The motile proportion was calculated as the fraction of mitochondria present in the first image of a set that showed any displacement of >2μm between consecutive images over the subsequent 10 minutes of imaging. The proportion of mitochondria that were motile decreased significantly over the developmental period that we analyzed (figure 3B). For example, at 2 days post-fertilization (2dpf) 19.7 ± 2.6 % mitochondria were motile, whereas by 5dpf this had fallen to 10.5 ± 2.4% ($p<0.017$, z-test with Bonferroni correction). Further inspection of primary images showed that the majority of motile mitochondria showed exclusively unidirectional movement over the course of the imaging period. Calculation of the ratio of anterograde displacement to retrograde displacement over the course of multiple experiments confirmed that 90% of the total motile mitochondria showed more than tenfold displacement in one direction with respect to the other, with the remaining 10% motile mitochondria showing oscillatory movements or small displacements that reverted to the initial location in subsequent images (figure 3C). This distribution allowed us to assign mitochondria categorically as showing unidirectional anterograde or retrograde movement, defined as:

$$\text{Anterograde:}\quad \frac{\Sigma\,(\text{image- to- image anterograde displacements})}{\Sigma\,(\text{image- to- image retrograde displacements})} > 10 \qquad (1)$$

$$\text{Retrograde:}\quad \frac{\Sigma\,(\text{image- to- image anterograde displacements})}{\Sigma\,(\text{image- to- image retrograde displacements})} < 0.1 \qquad (2)$$

Overall, anterograde movement predominated such that 60% of mitochondria with unidirectional motility at 2, 3 and 5 dpf moved in a rostrocaudal direction. Relative to 2 and 3 dpf, both anterograde and retrograde mitochondrial movement declined at 4 and 5 dpf, but with a relatively larger reduction in anterograde movement at 4 dpf (figure 4A, D).

We next calculated the velocity of mitochondrial movement (figure 4B, E). We analyzed retrograde and anterograde movements separately to determine if the different molecular mechanisms underlying antero- and retrograde transport are associated with different transport speeds. Velocity for an individual mitochondrion was calculated as:

$$\text{Velocity} = \frac{\Sigma\,(\text{image- to- image displacements in relevant direction})}{(\text{number of displacements in relevent direction}) \times (\text{time period between images})} \quad (3)$$

Overall, average mitochondrial velocity did not change significantly over development, although retrograde velocity was consistently slightly faster than anterograde velocity; thus, mean anterograde velocities varied between 0.59 μm/s to 0.65 μm/s at different developmental points, whereas mean retrograde velocity varied between 0.67 μm/s and 0.71 μm/s.

Finally, mitochondria were frequently seen to show periods of movement interspersed with pauses. In order to quantify this observation, for each mitochondrion we determined the proportion of transitions between consecutive images at which displacement exceeded threshold (% time motile; figure 4C, F). We found significant changes in the proportion of time mitochondria were motile during development, with more frequent pauses being apparent at earlier time points. For example, at 2 dpf, mitochondria undergoing anterograde transport showed displacement at a mean of 53.9 ± 3.0 % image transitions, whereas by 3dpf this had increased to 78.1 ± 1.6%. There was no statistically significant difference in % time motile between mitochondria that were undergoing anterograde versus retrograde transport, although the proportion was consistently slightly higher for anterograde transport.

Together these data show that mitochondrial transport can be quantified in CNS dopaminergic neurons of live zebrafish. Although there was substantial variability in the measured parameters, by sampling a large number of mitochondria the following trends could be detected: (i) a higher proportion of mitochondria was motile at earlier larval time points; (ii) motile mitochondria at earlier time points showed less continuous movement; (iii) anterograde transport predominated during early development; and (iv) retrograde transport may be slightly faster and less continuous than anterograde transport.

Establishment of a pre-symptomatic PD model in larval zebrafish

We next sought to determine whether changes in mitochondrial motility in dopaminergic neurons could be detected in a pre-symptomatic model of PD, as an early event prior to the onset of neurodegeneration. Inhibition of mitochondrial complex I function in dopaminergic neurons using the toxicant MPP^+, which is selectively transported into dopaminergic neurons, is routinely used in several different species (including zebrafish) to replicate features of PD, including: mitochondrial dysfunction; oxidative damage to cellular components; consumption of endogenous antioxidants; neurochemical deficits; motor

abnormalities that are reversed by pharmacological agents that promote dopaminergic function; and degeneration of dopamine neurons.

We and others have previously shown that exposure to 0.5 – 1.0mM MPP^+ over 3 – 5 days causes degeneration of dopaminergic neurons, neurochemical deficits and motor abnormalities in larval zebrafish (Farrell et al., 2011; Sallinen et al., 2009). In order to establish a pre-symptomatic model to study the early effects of MPP^+ on mitochondrial transport in dopaminergic neurons, we exposed larval zebrafish to lower concentrations of MPP^+, and for shorter time periods than previously used to cause loss of dopaminergic neurons (figure 5A). Larval zebrafish exposed to 0.5 or 1.0mM MPP^+ for 16 hours from 4dpf to 5dpf, showed no difference in survival (figure 5B), morphology (figure 5C), or heart rate (figure 5D) compared with controls. By whole mount immunofluorescence and exhaustive counts of TH-expressing cells in the telencephalon (figure 5E), pretectal region (figure 5F) and diencephalon (figure 5G) of larval zebrafish, we established there was no loss of dopaminergic neurons in any CNS group following MPP^+ exposure for 16 hours (figure 5H – N). We next measured neurotransmitter levels by HPLC. Although MPP^+-exposed larvae showed a trend towards modestly decreased whole-animal dopamine levels, this was not statistically significant (figure 6A). There was no difference in 5HT levels between MPP^+ exposed larvae and controls (figure 6B). Finally, we evaluated motor function in a 96-well plate spontaneous motility assay that we have previously shown to be sensitive to loss of dopaminergic function. There were no detectable motor deficits after exposure to MPP^+ at 0.5 or 1.0mM for 16 hours compared with controls (figure 6C – H). Together, these data show that exposure of larval zebrafish to 0.5mM or 1.0mM MPP^+ for 16 hours (the time point at which mitochondrial transport was assessed below) did not cause systemic toxicity, motor dysfunction or loss of dopaminergic neurons, but may have caused a modest decrease in total dopamine levels.

After longer exposure, we observed dose-dependent motor deficits (supplemental figure 2). Thus, following a second 16hr period of exposure, both 0.5mM and 1mM MPP^+ decreased zebrafish mobility, but the effect was significantly more severe in the 1mM MPP+ group (mean velocity for control zebrafish 1.28±0.21 mm/s, compared with 0.77±0.08 mm/s following 2 × 16 hour exposures of 0.5mM MPP^+, or 0.54±0.05 mm/s following 1.0mM MPP^+; $p<0.0001$, 0.5 or 1.0mM MPP^+ compared with control; $p<0.05$, 0.5mM versus 1mM MPP^+, 1-way ANOVA). These data confirm that early dose-dependent pathogenic events in dopaminergic neurons occurring after the first 16-hour MPP^+ exposure precede the onset of neuronal dysfunction underlying motor deficits and that the higher concentration of MPP+ causes more severe damage to dopaminergic neurons.

Mitochondrial flux reversal in dopaminergic neurons is an early event following MPP^+ exposure

We next asked whether mitochondrial transport is altered in dopaminergic neurons *in vivo*, in our pre-symptomatic larval zebrafish MPP^+ model. *roy*$^{-/-}$; *nacre*$^{-/-}$; Tg(*otpb:gal4*); Tg(*UAS:mtPAGFP:mtDsRed2*) zebrafish were exposed to MPP^+ or vehicle for 16 hours, then mitochondrial transport was analyzed in dopaminergic axons as described above to

determine the proportion of motile mitochondria, their direction of transport, and their velocity and proportion of time moving.

After exposure to 0.5mM MPP^+, the percentage of total axonal mitochondria that were motile significantly increased (figure 7A). In control animals exposed to vehicle only, 12.9 ± 2.3% total mitochondria were found to be motile, whereas 19 ± 1.7% mitochondria were motile after exposure to 0.5mM MPP^+ (control versus 0.5mM MPP^+, $p<0.017$, z-test with Bonferroni correction). In contrast, mitochondrial movement was strikingly decreased after exposure to 1.0mM MPP^+ treatment, so that only 5.5 ± 1.3% of total mitochondria showed any movement (control versus 1.0mM MPP^+, $p<0.017$, z-test with Bonferroni correction).

The directionality of mitochondrial transport showed dramatic changes following MPP^+ exposure (figure 7B, E, F). Using the same definitions for anterograde and retrograde transport as shown above, there was an almost 3-fold increase in the proportion of mitochondria undergoing retrograde axonal transport in the 0.5mM MPP^+ group with respect to controls (control 2.6 ± 0.5% versus 0.5mM MPP^+ 7.5 ± 1.5%, $p<0.017$, z-test with Bonferroni correction; figure 7B). This was accompanied by a trend towards decreased anterograde axonal transport in the 0.5mM MPP^+ group with respect to controls (control 6.1% ± 0.8% versus 0.5mM MPP^+ 4.4% ± 1.1%; figure 7F). Consequently the anterograde-preponderant mitochondrial flux observed in control animals (retrograde/anterograde ratio) was reversed to become strongly retrograde-dominant (retrograde/anterograde ratio: 0.4 in control group versus 1.7 in 0.5mM MPP^+ group; figure 7E).

In contrast, exposure to 1.0mM MPP^+ significantly reduced transport overall (figure 7A). Consequently, the proportion of mitochondria undergoing anterograde movement was significantly decreased (control 6.1% ± 0.8 versus 1.0mM MPP+ 1.4% ± 0.6%, $p<0.017$, z-test with Bonferroni correction; figure 7F) and there was a trend towards reduced retrograde transport also (control 2.6% ± 0.5% versus 1.0mM MPP+ 1.2% ± 0.6%; figure 7B). The loss of anterograde transport was disproportionately high such that, similar to 0.5mM MPP^+ exposure, the retrograde/anterograde ratio was elevated with respect to baseline (figure 7E). In addition, an increased number of mitochondria showed motility but no net transport following 1.0mM MPP^+ exposure. Many of these mitochondria showed multiple directional reversals, suggesting severe dysregulation of mitochondrial transport.

Despite these dramatic changes in directionality, other aspects of mitochondrial transport showed only modest differences following exposure to these low concentrations of MPP^+. The velocity of retrograde mitochondrial transport was unchanged at any concentration of MPP^+ (figure 7C), whereas mean anterograde transport velocity was significantly reduced following exposure to 0.5mM MPP^+ (figure 7G). There were no significant differences in the proportion of time that motile mitochondria were moving at any concentration of MPP^+ (figure 7D, H).

Together, these data show that subacute exposure to low concentrations of the mitochondrial complex I inhibitor MPP^+ induced dramatic changes in mitochondrial transport, including a reversal in net flux from anterograde-preponderant to retrograde-preponderant transport;

these changes preceded any detectable abnormalities of neurochemistry, behavior or dopaminergic neuronal morphology or survival.

Discussion

Our new zebrafish lines and imaging methods allowed us to measure mitochondrial transport in dopaminergic neurons of the intact CNS for the first time. These data are important, because they provide direct evidence *in vivo* that dramatic changes in mitochondrial transport precede other markers of pathogenesis in a model of pre-symptomatic PD, suggesting that altered mitochondrial dynamics may be a proximate event and potentially a therapeutic target.

Imaging mitochondrial dynamics in CNS dopaminergic neurons in vivo

We and others have previously detected early changes in mitochondrial dynamics of cultured neurons following exposure to toxicants implicated in PD pathogenesis (Arnold et al., 2011; Kim-Han et al., 2011; Lu et al., 2014). However, the restriction of prior studies to cultured cells is a significant weakness. PD pathogenesis is selective, but the cell-autonomous and non-autonomous factors that define disease-susceptibility are largely unknown and consequently have not yet been replicated *in vitro*. Furthermore, the use of an *in vivo* model allows correlation of imaging data with key functional aspects such as motor behavior, and provides the opportunity to carry out studies in neurons with physiological connectivity and synaptic activity, glial contact, and CNS microenvironment. Although inferences about mitochondrial dynamics have been made from imaging human and animal-derived tissue samples using static modalities, our prior work *in vitro* showed that static endpoints correlate poorly with a range of indices that can be measured directly by dynamic imaging (Arnold et al., 2011; Berman et al., 2009). Consequently, the development of a model that allows direct observation of mitochondria in dopaminergic neurons in the vertebrate CNS is a significant advance.

Dynamic imaging of mitochondria in live zebrafish has been reported previously in cells of the somites and pharyngeal arches during early development (Kim et al., 2008), and in primary sensory Rohon-Beard neurons (O'Donnell et al., 2014; Plucinska et al., 2012). Imaging these superficially-located cell populations is less challenging than the deeply-located CNS dopaminergic neurons that are relevant to PD. Transgenic zebrafish expressing mitochondrially-targeted mCherry in dopaminergic neurons under regulatory elements from the *slc6a3* (dopamine transporter) were reported recently (Noble et al., 2015), but dynamic imaging was not carried out. Confocal imaging of CNS axons presents a number of difficulties, including the non-linear vectors of axonal projections, significant tissue thickness and signal attenuation, and embryo pigmentation. Analysis of the resulting images, which include a large number of stationary and motile mitochondria, is also non-trivial. We addressed these challenges by: imaging a dopaminergic tract in which axons are closer to the surface of the animal and run an approximately linear course; employing a mutant background that lacks pigment; using high-end imaging technology with enhanced sensitivity to detect the signal from fluorescent proteins; and verifying mitochondrial tracking manually. Our methodology will allow subsequent studies to determine the role of

mitochondrial transport in the early pathogenic events that follow other genetic or environmental perturbations mimicking etiological factors implicated in PD. In addition, the inclusion of photoactivatable GFP in our bidirectional UAS construct will permit subsequent studies to investigate mitochondrial fission and fusion directly.

Development of mitochondrial transport in dopaminergic neurons

Our initial studies using this new model characterized how mitochondrial axonal transport changes in the axons of CNS dopaminergic neurons during development. Overall, earlier in development, the proportion of mobile mitochondria was higher, anterograde transport was more prevalent, and transport was less continuous. Mitochondria have previously been shown to migrate toward, and remain in, cellular locations of highest ATP demand (Hollenbeck and Saxton, 2005; Morris and Hollenbeck, 1993). The earliest descending dopaminergic growth cones in zebrafish were previously demonstrated within the rostral spinal cord at 16 – 24 hours post-fertilization; by 2dpf, dopaminergic axons were seen in the ventrolateral spinal cord along its entire rostro-caudal length (McLean and Fetcho, 2004a). Tracing studies showed that these axons were derived from ventral diencephalic dopaminergic neurons and by 4dpf appeared to make contacts with primary motor neurons (McLean and Fetcho, 2004b). Subsequent physiological and ablation experiments showed that the dopaminergic diencephalospinal projection mediates a critical developmental switch in motor behavior between 3dpf and 4dpf (Lambert et al., 2012; Thirumalai and Cline, 2008). Our observations on mitochondrial transport consequently span the developmental window during which dopaminergic diencephalospinal axons are growing, forming synapses and establishing functional circuits. We speculate that the elevated overall motility and preponderance of anterograde transport that we observed at 2dpf are related to the bulk transport of new mitochondria from the cell body to regions that are developing high metabolic demand, for example growth cones and nascent synapses. We further speculate that later in development, the less frequent transport we observed represents replacement of selected damaged mitochondria from the distal axon or synaptic terminals with new mitochondria from the cell body.

Mitochondrial transport along microtubules is ATP-dependent and relies on the molecular motor proteins kinesin (anterograde) and dynein (retrograde) (Saxton and Hollenbeck, 2012). Mitochondrial transport velocities in our study were unchanged through development and the values we measured are compatible with those determined in other experimental systems (Ligon and Steward, 2000). We also found that retrograde transport was overall modestly faster than anterograde transport, similar to data reported previously in peripheral nerve (Misgeld et al., 2007) and suggesting that the transport speed is primarily determined by the properties of the relevant molecular motor.

MPP^+ provokes changes in mitochondrial transport prior to other detectable pathogenic changes

MPP^+ is actively transported by the dopamine transporter into dopaminergic terminals, where it inhibits complex I of the mitochondrial electron transport chain. Its precursor MPTP caused acute Parkinsonism in a small number of patients (Langston et al., 1983). Both MPTP and MPP^+ have been used to provoke Parkinson’s disease pathology in a

number of different cell culture and animal models, including zebrafish. These models reproduce many of the morphological, biochemical, neurochemical and neurobehavioral features of PD. In the present work, we defined an MPP^+ exposure paradigm that did not provoke systemic toxicity, dopaminergic neuronal loss, neurobehavioral or neurochemical deficits. Even after these low-level subacute exposures, we detected dramatic changes in mitochondrial transport.

Similar to work reported previously in cultured mouse mesencephalic neurons (Kim-Han et al., 2011) or immortalized rat phaeochromocytoma cells (Cartelli et al., 2010), we observed a decrease in overall mitochondrial motility in zebrafish dopaminergic neurons *in vivo* after exposure to a higher concentration of MPP^+ (1.0mM). In contrast, a lower concentration of MPP^+ (0.5mM) caused an increase in overall motility, which has not been reported previously. Furthermore at this lower MPP^+ concentration, we observed a dramatic alteration in the directionality of mitochondrial transport; the overall increase in motility was accounted for by a three-fold increase in the frequency of mitochondria undergoing retrograde transport with respect to controls, whereas there was an accompanying reduction in anterograde transport. These data are in agreement with our previous *in vitro* study that showed an increase in retrograde mitochondrial transport in primary cortical neurons exposed chronically to low concentrations of the mitochondrial complex I inhibitor rotenone (Arnold et al., 2011). Similarly, cultured dorsal root ganglion cells in vitro showed an increase in retrograde mitochondrial transport following acute exposure to the Complex III inhibitor antimycin A (Miller and Sheetz, 2004) and squid axons exposed to low concentrations of MPP^+ also showed elevated mitochondrial transport (Morfini et al., 2007). Damaged mitochondria are thought to be transported back to the cell body for degradation by mitophagy. It is known that mitochondria with lower transmembrane potential are more likely to be transported towards the cell body (Miller and Sheetz, 2004). MPP^+ uptake and concentration into the terminals of dopaminergic neurons is likely to lead to mitochondrial depolarization, as has been shown by many others *in vitro* (e.g. Lambert and Bondy, 1989; Nakai et al., 2003). Retrograde transport of depolarized mitochondria may be particularly important in dopaminergic neurons, since mutations in proteins that link mitochondrial depolarization to their degradation (PINK1 and Parkin) cause recessive Parkinsonism (Narendra et al., 2008; Narendra et al., 2010). In addition, mitochondrial transport was recently found to be altered in larval segmental neurons from *Drosophila* lacking PINK1 (Devireddy et al., 2015), although dopaminergic neurons were not evaluated. Our working model is that MPP^+ uptake and concentration causes damage to mitochondria in dopaminergic terminals. At low levels of exposure, and early in the course of the response, enhanced retrograde transport is a compensatory mechanism that removes compromised mitochondria that may be a source of harmful reactive oxygen species from presynaptic terminals, and transports them to the cell body for degradation. At higher MPP^+ concentrations, cellular bioenergetics may be sufficiently impaired that transport in general is down-regulated. An alternative explanation – that microtubule function was impaired at higher MPP^+ concentrations (Cartelli et al., 2010) – seems less likely, since the transport velocity and % time moving did not change. Methodology is not yet available to directly assess mitochondrial depolarization, oxidative damage, ATP depletion and other similar parameters *in vivo*. Availability of relevant methods that are compatible with live imaging in

zebrafish larvae would enable us to further dissect the mechanisms underlying our observations and to test our working model directly.

In conclusion, our study is the first to demonstrate consistent changes in mitochondrial transport in DA neurons of an intact vertebrate *in vivo* following exposure to a PD-relevant toxicant. The findings are supportive of a potential role for mitochondrial dynamics early in PD neuropathology, since we observed robust changes in mitochondrial transport prior to later signs of damage and dysfunction in dopamine neurons. It will be of critical importance to determine which changes are compensatory and which are pathogenic, in order to identify opportunities for therapeutic intervention.

Supplementary Material

Refer to Web version on PubMed Central for supplementary material.

Acknowledgements

We thank Gretchen Blasko and David Grainy at the University of Pittsburgh Department of Laboratory Animal Resources for care of our zebrafish. This work was supported by research grants from the Parkinson's Disease Foundation (PDF-1RG-1104), the National Institutes of Health (ES022644, NS077954, and MH100008), and by a SPRIG award from the University of Pittsburgh Aging Institute.

References

Arnold B, et al. Integrating multiple aspects of mitochondrial dynamics in neurons: age-related differences and dynamic changes in a chronic rotenone model. Neurobiol Dis. 2011; 41:189–200. [PubMed: 20850532]

Asakawa K, et al. Genetic dissection of neural circuits by Tol2 transposon-mediated Gal4 gene and enhancer trapping in zebrafish. Proc Natl Acad Sci U S A. 2008; 105:1255–60. [PubMed: 18202183]

Bai Q, Burton EA. Cis-acting elements responsible for dopaminergic neuron-specific expression of zebrafish slc6a3 (dopamine transporter) in vivo are located remote from the transcriptional start site. Neuroscience. 2009; 164:1138–51. [PubMed: 19755139]

Bai Q, et al. Generation of a transgenic zebrafish model of Tauopathy using a novel promoter element derived from the zebrafish eno2 gene. Nucleic Acids Res. 2007; 35:6501–16. [PubMed: 17897967]

Bai Q, et al. Zebrafish DJ-1 is evolutionarily conserved and expressed in dopaminergic neurons. Brain Res. 2006; 1113:33–44. [PubMed: 16942755]

Bai Q, et al. Different mechanisms regulate expression of zebrafish myelin protein zero (P0) in myelinating oligodendrocytes and its induction following axonal injury. J Biol Chem. 2014; 289:24114–28. [PubMed: 25028515]

Barsoum MJ, et al. Nitric oxide-induced mitochondrial fission is regulated by dynamin-related GTPases in neurons. EMBO J. 2006; 25:3900–11. [PubMed: 16874299]

Berman SB, et al. Bcl-x L increases mitochondrial fission, fusion, and biomass in neurons. J Cell Biol. 2009; 184:707–19. [PubMed: 19255249]

Burte F, et al. Disturbed mitochondrial dynamics and neurodegenerative disorders. Nat Rev Neurol. 2015; 11:11–24. [PubMed: 25486875]

Cario CL, et al. Automated measurement of zebrafish larval movement. J Physiol. 2011; 589:3703–8. [PubMed: 21646414]

Cartelli D, et al. Microtubule dysfunction precedes transport impairment and mitochondria damage in MPP+ -induced neurodegeneration. J Neurochem. 2010; 115:247–58. [PubMed: 20649848]

Deng H, et al. The Parkinson's disease genes pink1 and parkin promote mitochondrial fission and/or inhibit fusion in Drosophila. Proc Natl Acad Sci U S A. 2008; 105:14503–8. [PubMed: 18799731]

Devireddy S, et al. The Organization of Mitochondrial Quality Control and Life Cycle in the Nervous System In Vivo in the Absence of PINK1. J Neurosci. 2015; 35:9391–401. [PubMed: 26109662]

Distel M, et al. Optimized Gal4 genetics for permanent gene expression mapping in zebrafish. Proc Natl Acad Sci U S A. 2009; 106:13365–70. [PubMed: 19628697]

Exner N, et al. Loss-of-function of human PINK1 results in mitochondrial pathology and can be rescued by parkin. J Neurosci. 2007; 27:12413–8. [PubMed: 17989306]

Farrell TC, et al. Evaluation of spontaneous propulsive movement as a screening tool to detect rescue of Parkinsonism phenotypes in zebrafish models. Neurobiol Dis. 2011; 44:9–18. [PubMed: 21669287]

Flinn L, et al. Complex I deficiency and dopaminergic neuronal cell loss in parkin-deficient zebrafish (Danio rerio). Brain. 2009; 132:1613–23. [PubMed: 19439422]

Flinn LJ, et al. TigarB causes mitochondrial dysfunction and neuronal loss in PINK1 deficiency. Ann Neurol. 2013; 74:837–47. [PubMed: 24027110]

Fujimoto E, et al. Identification of a dopaminergic enhancer indicates complexity in vertebrate dopamine neuron phenotype specification. Dev Biol. 2011; 352:393–404. [PubMed: 21276790]

Haddad D, Nakamura K. Understanding the susceptibility of dopamine neurons to mitochondrial stressors in Parkinson's disease. FEBS Lett. 2015; 589:3702–13. [PubMed: 26526613]

Hollenbeck PJ, Saxton WM. The axonal transport of mitochondria. J Cell Sci. 2005; 118:5411–9. [PubMed: 16306220]

Karbowski M, et al. Quantitation of mitochondrial dynamics by photolabeling of individual organelles shows that mitochondrial fusion is blocked during the Bax activation phase of apoptosis. J Cell Biol. 2004; 164:493–9. [PubMed: 14769861]

Kawakami K, et al. A transposon-mediated gene trap approach identifies developmentally regulated genes in zebrafish. Dev Cell. 2004; 7:133–44. [PubMed: 15239961]

Kim-Han JS, et al. The parkinsonian mimetic, MPP+, specifically impairs mitochondrial transport in dopamine axons. J Neurosci. 2011; 31:7212–21. [PubMed: 21562285]

Kim MJ, et al. Real-time imaging of mitochondria in transgenic zebrafish expressing mitochondrially targeted GFP. Biotechniques. 2008; 45:331–4. [PubMed: 18778258]

Kitada T, et al. Mutations in the parkin gene cause autosomal recessive juvenile parkinsonism. Nature. 1998; 392:605–8. [PubMed: 9560156]

Lam CS, et al. Zebrafish embryos are susceptible to the dopaminergic neurotoxin MPTP. Eur J Neurosci. 2005; 21:1758–62. [PubMed: 15845104]

Lambert AM, et al. The conserved dopaminergic diencephalospinal tract mediates vertebrate locomotor development in zebrafish larvae. J Neurosci. 2012; 32:13488–500. [PubMed: 23015438]

Langston JW, et al. Chronic Parkinsonism in humans due to a product of meperidine-analog synthesis. Science. 1983; 219:979–80. [PubMed: 6823561]

Ligon LA, Steward O. Movement of mitochondria in the axons and dendrites of cultured hippocampal neurons. J Comp Neurol. 2000; 427:340–50. [PubMed: 11054697]

Lu X, et al. The Parkinsonian mimetic, 6-OHDA, impairs axonal transport in dopaminergic axons. Mol Neurodegener. 2014; 9:17. [PubMed: 24885281]

Lutz AK, et al. Loss of parkin or PINK1 function increases Drp1-dependent mitochondrial fragmentation. J Biol Chem. 2009; 284:22938–51. [PubMed: 19546216]

McKinley ET, et al. Neuroprotection of MPTP-induced toxicity in zebrafish dopaminergic neurons. Brain Res Mol Brain Res. 2005; 141:128–37. [PubMed: 16209898]

McLean DL, Fetcho JR. Ontogeny and innervation patterns of dopaminergic, noradrenergic, and serotonergic neurons in larval zebrafish. J Comp Neurol. 2004a; 480:38–56. [PubMed: 15515022]

McLean DL, Fetcho JR. Relationship of tyrosine hydroxylase and serotonin immunoreactivity to sensorimotor circuitry in larval zebrafish. J Comp Neurol. 2004b; 480:57–71. [PubMed: 15514919]

Milanese C, et al. Hypokinesia and reduced dopamine levels in zebrafish lacking beta- and gamma1-synucleins. J Biol Chem. 2012; 287:2971–83. [PubMed: 22128150]

Miller KE, Sheetz MP. Axonal mitochondrial transport and potential are correlated. J Cell Sci. 2004; 117:2791–804. [PubMed: 15150321]

Misgeld T, et al. Imaging axonal transport of mitochondria in vivo. Nat Methods. 2007; 4:559–61. [PubMed: 17558414]

Morfini G, et al. 1-Methyl-4-phenylpyridinium affects fast axonal transport by activation of caspase and protein kinase C. Proc Natl Acad Sci U S A. 2007; 104:2442–7. [PubMed: 17287338]

Morris RL, Hollenbeck PJ. The regulation of bidirectional mitochondrial transport is coordinated with axonal outgrowth. J Cell Sci. 1993; 104(Pt 3):917–27. [PubMed: 8314882]

Narendra D, et al. Parkin is recruited selectively to impaired mitochondria and promotes their autophagy. J Cell Biol. 2008; 183:795–803. [PubMed: 19029340]

Narendra DP, et al. PINK1 is selectively stabilized on impaired mitochondria to activate Parkin. PLoS Biol. 2010; 8:e1000298. [PubMed: 20126261]

Noble S, et al. Transgenic Zebrafish Expressing mCherry in the Mitochondria of Dopaminergic Neurons. Zebrafish. 2015; 12:349–56. [PubMed: 26355474]

O'Donnell KC, et al. Axon degeneration and PGC-1alpha-mediated protection in a zebrafish model of alpha-synuclein toxicity. Dis Model Mech. 2014; 7:571–82. [PubMed: 24626988]

Patterson GH, Lippincott-Schwartz J. A photoactivatable GFP for selective photolabeling of proteins and cells. Science. 2002; 297:1873–7. [PubMed: 12228718]

Plucinska G, et al. In vivo imaging of disease-related mitochondrial dynamics in a vertebrate model system. J Neurosci. 2012; 32:16203–12. [PubMed: 23152604]

Poole AC, et al. The PINK1/Parkin pathway regulates mitochondrial morphology. Proc Natl Acad Sci U S A. 2008; 105:1638–43. [PubMed: 18230723]

Rink E, Wullimann MF. The teleostean (zebrafish) dopaminergic system ascending to the subpallium (striatum) is located in the basal diencephalon (posterior tuberculum). Brain Res. 2001; 889:316–30. [PubMed: 11166725]

Rink E, Wullimann MF. Development of the catecholaminergic system in the early zebrafish brain: an immunohistochemical study. Brain Res Dev Brain Res. 2002; 137:89–100. [PubMed: 12128258]

Sallinen V, et al. Dopaminergic cell damage and vulnerability to MPTP in Pink1 knockdown zebrafish. Neurobiol Dis. 2010; 40:93–101. [PubMed: 20600915]

Sallinen V, et al. MPTP and MPP+ target specific aminergic cell populations in larval zebrafish. J Neurochem. 2009; 108:719–31. [PubMed: 19046410]

Saxton WM, Hollenbeck PJ. The axonal transport of mitochondria. J Cell Sci. 2012; 125:2095–104. [PubMed: 22619228]

Scheer N, Campos-Ortega JA. Use of the Gal4-UAS technique for targeted gene expression in the zebrafish. Mech Dev. 1999; 80:153–8. [PubMed: 10072782]

Tanner CM, et al. Rotenone, paraquat, and Parkinson's disease. Environ Health Perspect. 2011; 119:866–72. [PubMed: 21269927]

Tay TL, et al. Comprehensive catecholaminergic projectome analysis reveals single-neuron integration of zebrafish ascending and descending dopaminergic systems. Nat Commun. 2011; 2:171. [PubMed: 21266970]

Thirumalai V, Cline HT. Endogenous dopamine suppresses initiation of swimming in prefeeding zebrafish larvae. J Neurophysiol. 2008; 100:1635–48. [PubMed: 18562547]

Valente EM, et al. Hereditary early-onset Parkinson's disease caused by mutations in PINK1. Science. 2004; 304:1158–60. [PubMed: 15087508]

Van Laar VS, Berman SB. The interplay of neuronal mitochondrial dynamics and bioenergetics: implications for Parkinson's disease. Neurobiol Dis. 2013; 51:43–55. [PubMed: 22668779]

Wang X, et al. DLP1-dependent mitochondrial fragmentation mediates 1-methyl-4-phenylpyridinium toxicity in neurons: implications for Parkinson's disease. Aging Cell. 2011; 10:807–23. [PubMed: 21615675]

Wen L, et al. Visualization of monoaminergic neurons and neurotoxicity of MPTP in live transgenic zebrafish. Dev Biol. 2008; 314:84–92. [PubMed: 18164283]

White RM, et al. Transparent adult zebrafish as a tool for in vivo transplantation analysis. Cell Stem Cell. 2008; 2:183–9. [PubMed: 18371439]

Xi Y, et al. Transgenic zebrafish expressing green fluorescent protein in dopaminergic neurons of the ventral diencephalon. Dev Dyn. 2011; 240:2539–47. [PubMed: 21932324]

Zhou Y, et al. Quantification of larval zebrafish motor function in multiwell plates using open-source MATLAB applications. Nat Protoc. 2014; 9:1533–48. [PubMed: 24901738]

Highlights

- We generated transgenic zebrafish expressing florescent proteins in mitochondria
- Mitochondrial transport was imaged in the axons of dopaminergic neurons *in vivo*
- Developmental changes in transport correlated with axonal growth and synaptogenesis
- MPP^+ exposure caused a profound increase in retrograde transport
- These changes in transport preceded all other signs of pathogenesis

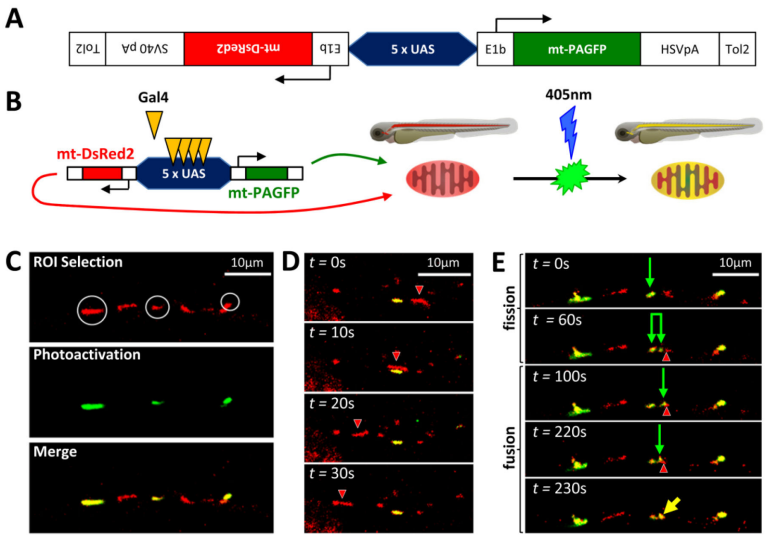

Figure 1. Bidirectional transgene construct enables observation of mitochondrial transport, fission and fusion in dopaminergic neurons *in vivo*

A: Schematic depiction of bidirectional transgene construct contained in plasmid pT2-5UAS:mtDsRed2:mtPAGFP

B: Illustration depicting transactivation of construct by Gal4, mitochondrial import and localization of products and photoactivation of mtPAGFP

C, D, E: *roy*$^{-/-}$; *nacre*$^{-/-}$; Tg(*otpb:gal4*); zebrafish embryos were microinjected with pT2-5UAS:mtPAGFP:mtDsRed2 and Tol2 mRNA at the single cell stage. At 3 dpf, single confocal planes were imaged through dopaminergic diencephalospinal axons expressing mtDsRed2 (red) and mtPAGFP (green). (C) Selection and photoactivation of GFP expression in single mitochondria. (D) Timelapse series showing transport of a mitochondrion (red; arrowhead) past a stationary mitochondrion (green). (E) Time-lapse series showing a mitochondrial fission event (green arrow shows parent mitochondrion; paired green arrows show daughter mitochondria), followed by a mitochondrial fusion event (green arrow and red arrowhead show individual mitochondria prior to fusion, yellow arrow shows resulting fusion product).

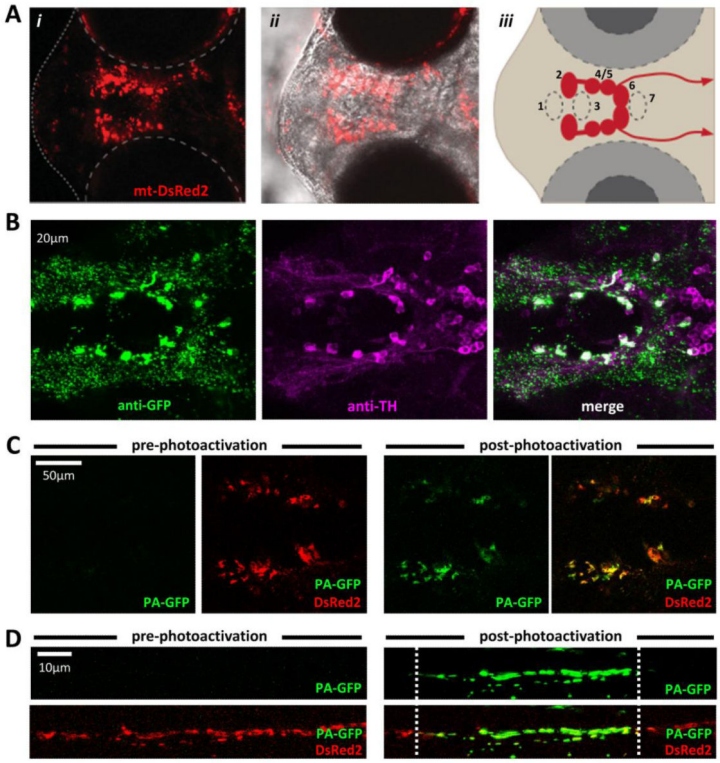

Figure 2. Stable transgenic zebrafish expressing mtDsRed2 and mtPAGFP in diencephalic dopaminergic neurons and their axons

A: Live imaging of a *roy*$^{-/-}$; *nacre*$^{-/-}$; Tg(*optb:gal4*); Tg(*UAS:mtPAGFP:mtDsRed2*) zebrafish at 3dpf. (i) mtDsRed2 fluorescence image; (ii) overlay with phase contrast image to show anatomical landmarks. (iii) schematic showing location and spinal projections of major diencephalic dopaminergic groups.

B: Confocal image of a whole mount *roy*$^{-/-}$; *nacre*$^{-/-}$; Tg(*optb:gal4*); Tg(*UAS:mtPAGFP:mtDsRed2*) zebrafish labeled with antibodies to GFP (green, left panel) and TH (magenta, middle panel), showing extensive co-localization between the two markers (white, right panel).

C, D: Live imaging of *roy*$^{-/-}$; *nacre*$^{-/-}$; Tg(*optb:gal4*); Tg(*UAS:mtPAGFP:mtDsRed2*) zebrafish at 3dpf verifying photoactivation of the mtPAGFP marker throughout the diencephalon (C) or along a specific axonal segment in the dopaminergic diencephalospinal projection (D).

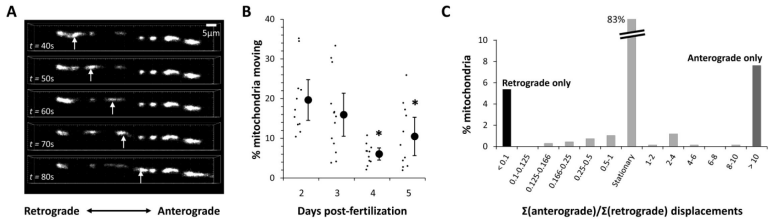

Figure 3. Identification and directional classification of mitochondrial transport in dopaminergic diencephalospinal axons during development

A: Time-lapse confocal series of a diencephalospinal axon in a live *roy*$^{-/-}$; *nacre*$^{-/-}$; Tg(*optb:gal4*); Tg(*UAS:mtPAGFP:mtDsRed2*) zebrafish. mtDsRed2 labeled mitochondria are seen distributed along the axon. Displacement of at least one mitochondrion between successive images is clearly seen in an anterograde direction (arrows; and see supplementary video 1).

B: Graph showing the proportion of mitochondria seen in the first frame of an image series that showed displacement over the subsequent 10 minutes of imaging. The proportion for each individual zebrafish (small markers) is shown alongside the mean and standard error for each developmental point (large markers with error bars). * denotes $p < 0.05$ compared with 2 dpf, z-test for proportions with Bonferroni correction.

C: Histogram showing the frequency distribution of the ratio of anterograde to retrograde displacements for individual mitochondria at 3 dpf. Most mitochondria were stationary over the 10 minutes of imaging, but motile mitochondria clearly showed unidirectional preference with displacement in one direction being 10-fold or more higher than the opposite direction.

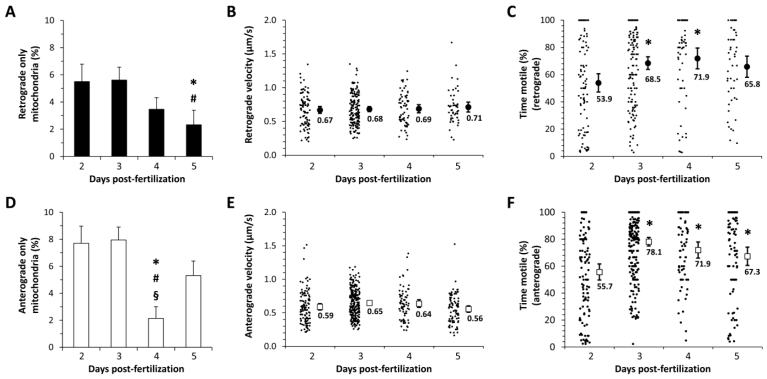

Figure 4. Quantification of mitochondrial direction, velocity and motility in dopaminergic diencephalospinal axons

The movements of mitochondria that showed >10-fold more retrograde displacement than anterograde ('retrograde'; panels A, B, C), or >10-fold more anterograde displacement than retrograde displacement ('anterograde; panels D, E, F), over the imaging period were analyzed separately.

A, D: Bar charts showing the proportion of all mitochondria imaged at each developmental point (2 – 5dpf) that showed either retrograde (A) or anterograde (D) transport. Error bars show standard error of the proportion. $p<0.05$ compared with *2dpf, $^{\#}$3dpf, or §5dpf, z-test for proportions with Bonferroni correction.

B, E: Retrograde (B) and anterograde (E) transport velocities are shown for individual mitochondria (small markers) along with the means for each developmental point (large markers). Error bars show the standard error of the mean.

C, F: The proportion of frame transitions during the imaging period at which there was significant displacement is shown for individual mitochondria (small markers) that underwent retrograde (C) or anterograde (F) transport. Mean values are shown for each developmental point (large markers). Error bars show the standard error of the mean. *$p<0.05$ compared 2dpf, one-way ANOVA with Tukey's *post hoc* test.

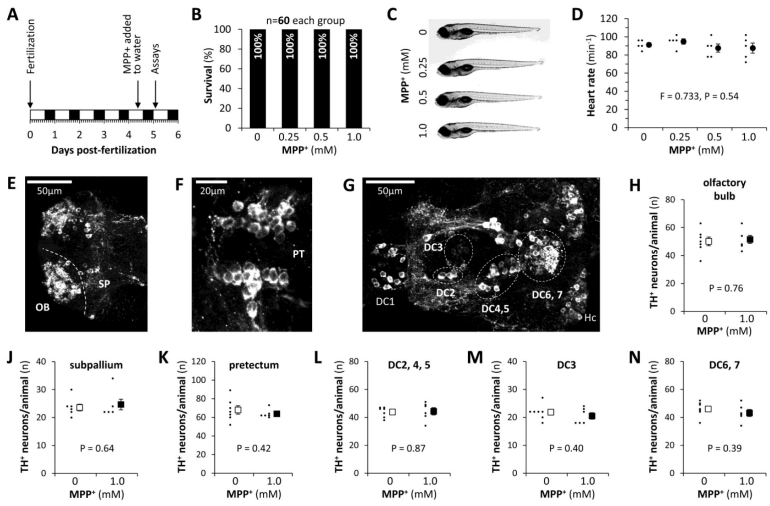

Figure 5. Survival, morphology and dopaminergic neuron counts in a presymptomatic zebrafish MPP$^+$ model of Parkinson's disease

A: Timeline for the subacute MPP$^+$ exposure paradigm used for the experiments shown in panels B – N and in figures 6 and 7. Wild-type zebrafish were exposed to MPP$^+$ at 4.5dpf and assays were carried out 16 hours later.

B: Bar chart showing zebrafish survival following subacute MPP$^+$ exposure.

C: Representative images of 5dpf wild-type zebrafish following subacute MPP$^+$ exposure.

D: Heart rates of 5dpf wild-type zebrafish treated with the indicated concentrations of MPP$^+$ as shown in panel A. The rates for five individual animals are shown (small markers) along with the mean for each MPP$^+$ concentration (large markers; error bars show standard error of the mean; data analyzed by one wat ANOVA).

E – G: Confocal Z-plane projections of whole mount 5dpf zebrafish brains labeled with an antibody to TH (white), showing the major dopaminergic neuronal groups of the (E) telencephalon, (F) pretectal region and (G) diencephalon. Key: OB, olfactory bulb; SP, subpallium; DC1 – 7, ventral diencephalic groups numbered according to the system proposed by Rink and Wullimann (Rink and Wullimann, 2002); Hc, caudal hypothalamus. Dotted lines show the boundaries between different groups.

H – N: Absolute exhaustive TH-immunoreactive neuronal counts of the groups shown in panels E – G. 6 control larvae (white markers) and 5 larvae that were exposed to the highest concentration of MPP$^+$ (1.0mM; black markers) were analyzed for each group. Each graph shows the total neuronal counts for individual larvae (small markers) and the mean for each experimental group (large markers; error bars show the standard error of the mean; data analyzed by unpaired T-test).

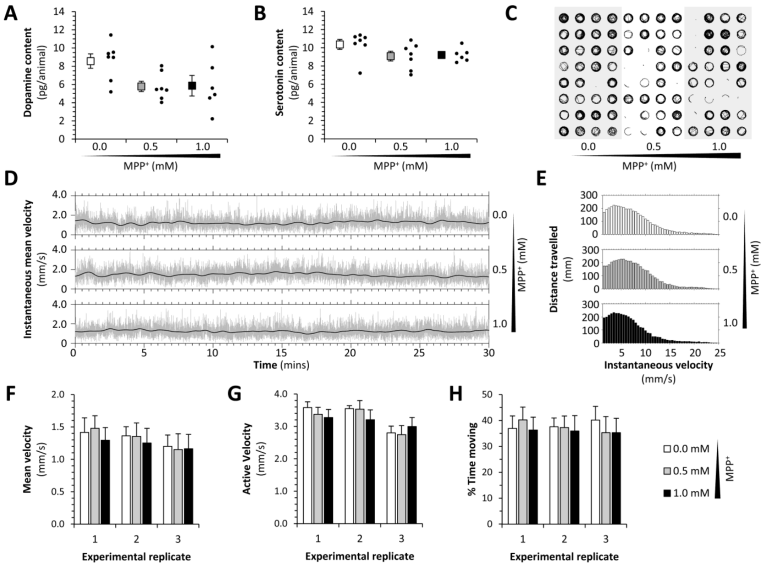

Figure 6. Neurochemistry and motor function in a presymptomatic zebrafish MPP$^+$ model of Parkinson's disease

A, B: Whole-animal neurotransmitter levels following exposure to MPP+. The graphs show dopamine (A) and serotonin (B) levels in lysates from 60 pooled larvae, expressed as pg neurotransmitter per larva. Individual experimental replicates are shown (small markers) along with the mean (large markers) for each concentration of MPP+, using the subacute paradigm shown in figure 5A. Error bars show standard error of the mean.

C – H: 96 zebrafish larvae were exposed to 0, 0.5 or 1.0mM MPP+ subacutely as shown in figure 5A. The larvae were then transferred to individual wells of a 96-well plate in fresh medium, and their movements measured by analysis of a video stream (Cario et al., 2011; Zhou et al., 2014). (C) Representative vector plot showing the centroid locus of each zebrafish in 1000 consecutive video frames at 4 frames/sec. (D) Instantaneous mean velocity plots for each experimental group over 30 minutes of recording. The light gray lines show the mean displacement of all larval centroids in each experimental group at each frame transition of video stream, scaled to indicate velocity. The black lines show the same data averaged over a moving 30-frame window. (E) Histograms showing the total displacement of the larval centroids over the entire 60-minute recording (y-axis) at each instantaneous velocity (x-axis); a separate histogram is shown for each experimental group. (F) Mean velocity (total displacement/measurement time period), active velocity (total displacement/time moving) and % time moving (time moving/measurement time period) are shown for each experimental group (white bars, control; gray bars, 0.5mM MPP+; black bars, 1.0mM MPP+). Three independent biological replicates (n=32 each group) are shown for each parameter. Bars show mean +/− standard error. Data analyzed using one-way ANOVA.

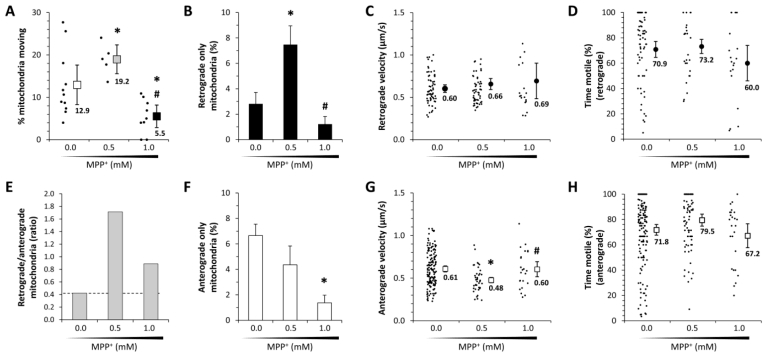

Figure 7. Mitochondrial flux reversal in a presymptomatic zebrafish MPP$^+$ model of Parkinson's disease

Zebrafish larvae were exposed to 0, 0.5 or 1.0mM MPP$^+$ subacutely as shown in figure 5A. Mitochondrial transport was then analyzed in their dopaminergic diencephalospinal axons as shown in figures 3 and 4.

A: Graph showing the proportion of mitochondria seen in the first frame of an image series that showed displacement over the subsequent 10 minutes of imaging. The proportion for each individual zebrafish (small markers) is shown alongside the mean for each concentration of MPP+ (large markers; error bars show standard error of the mean). $p<0.05$ compared with *0.0mM, $^{\#}$0.5mM, z-test for proportions with Bonferroni correction.

B, F: Bar charts showing the proportion of all mitochondria imaged following exposure to each concentration of MPP$^+$ that showed either retrograde (B; retrograde/anterograde displacements > 10) or anterograde (F; anterograde/retrograde displacements < 0.1) transport. Error bars show standard error of the proportion. $p<0.05$ compared with *0.0mM, $^{\#}$0.5mM, z-test for proportions with Bonferroni correction.

C, G: Retrograde (B) and anterograde (F) transport velocities are shown for individual mitochondria (small markers) along with the groups means (large markers; error bars show the standard error of the mean) following exposure to each concentration of MPP$^+$. $p<0.05$ compared with *0.0mM, $^{\#}$0.5mM, on-way ANOVA with Tukey's *post hoc* test.

D, H: The proportion of frame transitions during the imaging period at which there was significant displacement is shown for individual mitochondria (small markers) that underwent retrograde (D) or anterograde (H) transport. Mean values are shown following exposure to each concentration of MPP$^+$ (large markers; error bars show the standard error of the mean).

E: The ratio of mitochondria undergoing retrograde/anterograde transport is shown following exposure to each concentration of MPP$^+$, as a measure of directional flux. The baseline control value is indicated as a dotted line for comparison with other points.